Characterizing the heterogeneity of karst critical zone and its hydrological function: an integrated approach

Journal:	*Hydrological Processes*
Manuscript ID	HYP-18-0002.R1
Wiley - Manuscript type:	Special issue: Water in the Critical Zone
Date Submitted by the Author:	13-May-2018
Complete List of Authors:	Chen, Xi; State Key Laboratory of Hydrology-Water Resources and Hydraulic Engineering, Hohai University Zhang, Zhicai; Hohai University, State Key Laboratory of Hydrology-Water Resources and Hydraulic Engineering Soulsby, Chris; University of Aberdeen, School of Geosciences Cheng, Qin-Bo; Hohai University, College of Hydrology and Water Resources Binley, Andrew; Lancaster University, Lancaster Environment Centre Jiang, Rui; Hohai University, State Key Laboratory of Hydrology-Water Resources and Hydraulic Engineering Tao, Min; Hohai University, State Key Laboratory of Hydrology-Water Resources and Hydraulic Engineering
Keywords:	Cockpit karst, critical zone, hydrological functions, geophysical survey, tracers

Characterizing the heterogeneity of karst critical zone and its hydrological function: an integrated approach

Xi Chen[1,2*], Zhicai Zhang[2,3], Chris Soulsby[3], Qinbo Cheng[2,4], Andrew Binley[4], Rui Jiang[2], Min Tao[2]

1: Institute of Surface-Earth System Science, Tianjin University, Tianjin China
2: State Key Laboratory of Hydrology-Water Resources and Hydraulic Engineering, Hohai University, Nanjing 210098, China
3: School of Geosciences, University of Aberdeen, Aberdeen AB24 3UF, United Kingdom
4: Lancaster Environment Centre, Lancaster University, Lancaster, LA1 4YQ, United Kingdom

*Corresponding author E-mail: xichen@hhu.edu.cn

Submitted to Special issue: Water in the Critical Zone

Abstract

Spatial heterogeneity in the subsurface of karst environments is high, as evidenced by the multi-phase porosity of carbonate rocks and complex landform features that result in marked variability of hydrological processes in space and time. This includes complex exchange of various flows (e.g. fast conduit flows and slow fracture flows) in different locations. Here, we integrate various "state-of-the-art" methods to understand the structure and function of this poorly-constrained critical zone environment. Geophysical, hydrometric and tracer tools are used to characterize the hydrological functions of the cockpit karst critical zone in the small catchment of Chenqi, Guizhou province, China. Geophysical surveys, using electrical resistivity tomography (ERT), inferred the spatial heterogeneity of permeability in the epikarst and underlying aquifer. Water tables in depression wells in valley bottom areas, as well as discharge from springs on steeper hillslopes and at the catchment outlet, showed different hydrodynamic responses to storm event rainwater recharge and hillslope flows. Tracer studies using water temperatures and stable water isotopes (δD and $\delta^{18}O$) could be used alongside insights into aquifer permeability from ERT surveys to explain site- and depth-dependent variability in the groundwater response in terms of the degree to which "new" water from storm rainfall recharges and mixes with "old" pre-event water in karst aquifers. This integrated approach reveals spatial structure in the karst critical zone and provides a conceptual framework of hydrological functions across spatial and temporal scales.

Key words: Cockpit karst; critical zone; hydrological functions; geophysical survey; tracers; stable isotopes.

1 Introduction

Karst covers ~10% of the continents and about one quarter of the global population is completely or partially dependent on drinking water from karst aquifers (Ford and Williams, 2013). The southwest China karst region is one of the largest continuous karst areas, covering ~540×10^3 km^2 over eight provinces. The karst terrain displays a geomorphic transition as the topography gradually descends by 2,000 metres over 700 kilometres from the western Yunnan-Guizhou Plateau to the eastern Guangxi Basin. Cockpit karst is a specific geomorphology found in some tropical areas underlain by limestone formations. Conical hills and star shaped valleys are characteristic of such karst landscapes. Due to the distinct nature of karst geology and geomorphology in the humid tropics and subtropics, spatial heterogeneity in the subsurface is high, evidenced by specific landforms features (e.g. heavily fractured outcrops, sinkholes etc.) and complex subterranean conduit networks. This leads to highly dynamic variability of hydrological processes in space and time. This heterogeneity in karstic environments and their rapidly evolving nature makes them extremely vulnerable to natural and anthropogenic hazards. Hillslope springs and groundwater in valley bottom depressions in cockpit karst areas are the main water resources for local agriculture, industry and domestic use. However, the high hydrological variability results in vulnerability to the frequent occurrences of floods and droughts. Consequently, understanding the karst critical zone, its structures and hydrological functions in the southwest karst region of China is essential to mitigate natural disasters and adapt appropriate management strategies for sustainable water resource utilization.

Hydrological responses to rainfall in cockpit karst areas can be conceptualised as in Fig 1. The hydrological processes include rainfall infiltration in the soil and epikarst, water storage and flow in the transmissive zone, and hydrological connectivity between hillslope and depression units. To consider the effects of marked heterogeneity in the profile of the karst critical zone on hydrological function, the profile can be sub-divided into soil, epikarst, unsaturated and phreatic zones (Perrin et al., 2003). On the hillslope, since the permeability usually reduces with the depth (Williams, 1983) or less permeability layers underlie the epikarst zone, infiltrated water usually flows out as a spring. The phreatic zone is regarded as a transmissive zone through its well-developed conduit network (e.g. Emblanch et al., 2003; Perrin et al., 2003). Nevertheless, it is extremely heterogeneous in space. For example, the solutional conduits in karst aquifers connect with intergranular pores and fractures (often termed as matrix porosity), showing dual or even triple porosity zones (Worthington et al., 2017). Thus, karst aquifers are often conceptualized as dual porosity systems as residence times in the matrix are several orders of magnitude longer than those in the conduits (Goldscheider and Drew, 2007). However, even for the matrix porosity at a specific site, fracture apertures can widely vary, e.g. 0.01–0.1 mm (Long et al. 1982; Hyman et al. 2015); and for larger conduits, the density and connectivity with the surrounding fractures can vary greatly due to heterogeneity in the stratigraphy and geologic structure. Consequently, the characterization of the functioning of such complex systems remains a great challenge.

Hydrometric observations and tracer investigations are traditional and effective approaches to inferring flow processes within karst systems (Fig 1). Water table response is particularly sensitive to changes in hydrometeorological forcing because of the direct connectivity of the water table with the ground surface in surficial and shallow aquifers (Winter, 1999; Healy and Cook, 2002; Sophocleous, 2002; Lee et al., 2006). The water-table rise and fall during a specific storm period can be translated into a corresponding amount of groundwater recharge and discharge (Sophocleous, 1991; Xie and Yuan, 2010; Fan et al, 2014; Biswas et al, 2017). In karst areas, abundant springs on hillslopes and at catchment outlets reflect regional flow accumulation along conduits and underground channels. Spring hydrographs can be used to characterize karst systems (Kovacs and Perrochet, 2008) and better understand system behavior during floods (Winston and Criss, 2004) or droughts (Fiorillo, 2009).

As water flowing through soils or fractures carries sensible heat that can affect subsurface water temperatures on mixing (Anderson, 2005; Rau et al., 2014), distributed temperature measurements can provide excellent indications of flow and connectivity. Using water temperature as a tracer can thus help assess groundwater flow, groundwater-surface water exchanges (Becker et al., 2004; Niswonger et al., 2005; Lowry et al., 2007; Irvine et al, 2015), flow paths, mixing effects and residence times (Sun et al., 2016). This is especially useful in karst aquifers as fast flows overcome limitation of heat tracing at lower velocities (Rau et al., 2010, Rau et al., 2014). As rainwater may has different temperatures to groundwater, the arrival of new recharge at a karst spring is evidenced by changing water temperature (Ford and Williams, 2013). Subsurface temperature variability can thus be used to assess the degree of connectivity and relative importance of mixing (Hartmann et al., 2014; Mudarra et al., 2014).

Isotope studies have also substantially increased our understanding of detailed hydrological flow paths and mixing processes in the critical zone (Sprenger et al., 2017, 2018). Stable isotopes of water ($\delta^{18}O$ and $\delta^{2}H$) have also been widely used to provide insight into the functioning of karst systems (Barberá and Andreo, 2012; Mudarra and Andreo, 2011), the mixing of water from different sources (Aquilina et al., 2006; Plummer et al., 1998), and the their residence times (Batiot et al., 2003; Long and Putnam, 2004). Due to the high degree of variability of karst systems, continuous monitoring or event-based high-frequency sampling is essential, but logistically challenging (Goldscheider and Drew, 2007).

Hydrometric monitoring and tracer studies provide direct observations of hydro-dynamics which can indirectly hypothesize karst critical zone structures. However, explaining hydrological variability and identifying controls rely on detail information on karst hydrogeological properties in space. For example, Lee and Krothe (2001) used dissolved inorganic carbon (DIC) and δ^{13}DIC as tracers for conceptualizing hydrological functions using a four-component mixing model (rain, soil water, epikarstic water and diffuse phreatic water) for a karstic flow system. Similarly, Jiang et al. (2008) inferred runoff response thresholds in the epikarst by monitoring the spring's discharge, pH, electrical conductivity, temperature and rainfall. Increasingly, however, geophysical techniques are being used to provide more direct evidence about the geological setting of a karst system. Survey techniques, such as ground penetrating radar (GRP) and electrical resistivity tomography

(ERT), provide an efficient means of describing the karst structure, mapping karst conduits (Carrière et al., 2013; Martínez-Moreno et al., 2014) and defining the soil-rock interface (Chalikakis et al., 2011). Such geological evidence is crucial for delineating hydraulic structures, such as complex subsurface drainage networks in the karst which can link local fissure and fracture networks with the dominant large conduit systems (Chalikakis et al, 2011; Hartmann et al., 2014; Binley et al., 2015). These insights can be particularly powerful if geophysical approaches are integrated with hydrometric and tracer observations and at the same study site (e.g. Soulsby et al., 2016).

Different methodologies have advantages and limitations (see Goldscheider and Drew, 2007) so isolated measurements and observations are inadequate for characterizing a karst system. Although many researchers apply combinations of such methods for assessing the hydrology karst areas, they seldom integrate insights from multi-scale distributed geophysical surveys, hydrometric observations and tracer investigations. Consequently, in the southwest karst region of China, we lack a conceptual framework that characterizes spatial heterogeneity hydrological functioning at multiple scales and/or in different geographic regions.

The overall aim of this study was to integrate these approaches to visualize the complex heterogeneity in karst critical zone and its effect on hydrological functions. By so doing, the study will also help identify dominant processes to incorporate in the structure of hydrological models. We based the investigation in the long-term study site of Chenqi in the cockpit karst region of Guizhou province, southwest China. Our objectives were to: (1) undertake geophysical surveys using electrical resistivity tomography to characterize the structure of the karst critical zone and identify variations in the permeability which define fast and slow flow domains in karst aquifers. (2) Monitor groundwater levels in wells and discharge from hillslope springs and the catchment outlet to characterize the spatial and temporal variations of hydrodynamic response to rainfall events. (3) Use stable isotopes of water ($\delta^{18}O$ and $\delta^{2}H$) qualitatively understand how "new" event water from rainwater and "old" pre-event water from low permeability aquifers recharges mix and contribute to catchment discharge, particularly during heavy rainfall in the vertical profiles. Improved conceptualization of a dual flow system that accounts for local aquifer heterogeneity influences on the hydrological connection between fast and slow reservoirs is proposed.

2 Study area, data and methods

2.1 Study catchment

The study was focused in the small (1.2km^2) Chenqi catchment, located in the Puding Karst Ecohydrological Observation Station, Guizhou Province, southwest China (Fig. 2). It is a typical cockpit karst landscape, with surrounding conical hills separated by star shaped valleys. Surface elevation ranges from 1320m at the catchment outlet to a maximum of 1500 m. Geological strata in the basin include dolostone, thick and thin limestone, marlite and Quaternary soil (profiles of A-A' and B-B' in Fig 2). Limestone formations form the higher elevation areas with 150-200 m thickness, which lie above an impervious marlite formation. The Quaternary soils are irregularly developed on carbonate rocks and unevenly distributed, with outcrops of carbonate rocks covering 10-30% of the catchment. Dominant vegetation ranges from deciduous broad-leaved forest on the upper and middle parts of the steep hillslopes and corn and rice paddy at the low of the gentle hillslopes and depression.

The catchment is located in a region with a subtropical wet monsoon climate with mean annual temperature of 20.1^{o}C, highest in July and lowest in January. Annual mean precipitation is 1140 mm, almost all falling in a distinct wet season from May to September and a dry season from October to April next year. Average monthly humidity is high, ranging from 74% to 78%.

2.2 ERT survey in the valley depression

Electrical resistivity tomography (ERT) was used to survey the geological properties along five transects crossing the depression (Fig 3). The surveyed profiles were located adjacent to four observation wells (see below) and three sinkholes to identify the geological controls on groundwater dynamics. The surveys were carried out in spring 2017 using a Syscal Pro (Iris Instruments, France) resistivity meter with electrode spacing between 2 and 5m. We used a dipole-dipole electrode configuration (see for example, Binley, 2015) with dipole spacings of one, two and three times the electrode separation and up to 20 levels. The dipole-dipole configuration was selected to allow sensitivity of lateral variation in resistivity. Inversion of the ERT data was carried out using the code R2 (http://www.es.lancs.ac.uk/people/amb/Freeware/R2/R2.htm). The resulting composite ERT image is shown in Fig 3. The resistivity ranges from ~15 Ωm to ~8000 Ωm. Based on ERT surveys carried out adjacent to outcrops in neighbouring areas of the catchment we interpret the ERT results in Fig 3 as: (i) an upper layer consisting of moist soils or extensively fractured rock (resistivity <100 Ωm, blue in Fig. 3); (ii) carbonate rock with a high secondary porosity (and hence permeability) (100 Ωm < resistivity < 1000 Ωm, green/yellow in Fig. 3); (iii) an underlying carbonate rock with low secondary porosity and hence relatively low permeability (resistivity >1000 Ωm, red in Fig. 3).

The ERT image shows that the depression aquifer is highly heterogeneous in both the horizontal direction and vertical direction. Based on our interpretation of the ERT image: well W1 is surrounded by the less permeable aquifer (red colour) and its upper layer of carbonate rock appears particularly impermeable; wells W3 and W4 are located in the higher permeability area (blue colour); well W5 is located in the less permeable aquifer and its top soils (blue colour) and the carbonate rock in the upper layer (yellow colour) is relatively more permeable than that in the deep layer (red colour). The relatively permeable upper layer at W5 appears much thinner than those at other wells.

In a previous study, a GPR MALA Professional Explorer (ProEx) System was used for investigation of the fracture zone thickness on the hillslope. The epikarst thickness on the hillslope was identified to be in a range of 7.6~12.56 m. Along the hillslope, the thickness and the epikarst zone at the lower areas is deeper than in the upper areas (Zhang et al. 2013).

2.3 Hydrometric observations

In the Chenqi catchment, groundwater levels in the valley depression were routinely monitored at the four wells (W1, W3, W4 and W5) with depth to ground surface of 35, 23, 13 and 16 m, respectively. The well screening was installed over the whole depth for each of the wells to reflect local flow exchanges at various depths. Flows discharging from a hillslope spring (HS) at the foot of the eastern steep hillslope and leaving the catchment outlet were measured by v-notch weirs (Fig. 2). The water level and temperature at each well, the hillslope spring and the catchment were automatically recorded by HOBO U20 water level logger (Onset Corporation, USA) with a time interval of 15 minutes. Additionally, an automatic weather station was set on the upper hillslope to record precipitation, air temperature, and air humidity and pressure.

Data collection ran from 28 July 2016 to 30 October 2017. Hourly variations of rainfall, discharge from the hillslope spring and catchment outlet, as well as water levels in the four wells are shown in Fig 4, and their corresponding temperature are shown in Fig 5. Statistical characteristics of water levels, flow discharges and temperatures are summarized in Table 1 and Table 2.

2.4 Stable isotope analysis

For isotope analysis, the hillslope spring (HS), groundwater from outlet and rainfall were sampled at daily intervals during the wet season from June to August 2017. Additionally, they were intensively sampled during eight rainfall events in the wet season using an autosampler set to hourly intervals. Depression groundwater was sampled from the four wells during four rainfall events within the study period; in each event, water samples were collected before, during and after rainfall. At each well, water was sampled from multiple depths with a depth-specific sampler to give a profile of the isotopic composition of the groundwater column. All water samples (1695 replicates) were collected by 5 ml glass vials. The stable isotopic composition of δ^2H (δD) and $\delta^{18}O$ ratios were determined using the MAT 253 laser isotope analyser (the instrument precision ±0.5‰ for δ^2H and ±0.1‰ for $\delta^{18}O$). Isotope ratios are reported in the d-notation using the Vienna Standard Mean Ocean Water standards (Coplen, 1994). The analyzed results of the isotopic values are shown in Figs 6-8.

3 Results

3.1 Hydroclimatic and groundwater variability in the depression

Generally, the hydrometric observations reveal sharp rises and falls in water level at the four wells in response to rainfall events (Fig. 4). However, the magnitude of the water table response and the rate of the water table recessions exhibit differences at the four wells, which indicates spatial differences in the groundwater response to recharge and attenuation of the hydrograph. The magnitude of the temporal dynamic is larger and more attenuated at W3 and W4 in the low electrical resistivity (interpreted higher permeability) areas, and abrupt at W1 and W5 where particularly heavy rainfall is needed to produce a large water table rise. These differences are apparent in the coefficient of variation (CV) of water level data for W3 and W4 (0.21 and 0.61, respectively), whilst the CV of W1 and W5 is only 0.03 and 0.07, respectively (see Table 1).

Temporal variability in temperature clearly demonstrates that groundwater dynamics at W3 and W4 are more directly influenced by hydroclimate variability compared with W1 and W5 (Fig 5). The former wells show marked temperature excursions towards air temperatures in response to rainfall events, whilst the latter wells exhibit highly attenuated temperatures typical of deeper groundwater. As shown in Table 2, the CV of water temperature at W3 and

W4 is 0.026 and 0.036, while the CV of W1 and W5 is only 0.004 and 0.012, respectively. The sharp rise and drop of water temperature at W3 and W4 during rainfall is clearly consistent with the fast arrival of freshly infiltrated rainwater. In contrast, the limited seasonal fluctuation of water temperatures at W1 and W5 indicate little evidence of rainfall recharge consistent with the interpreted low permeability in the upper layers (high resistivity zone in Fig 3).

As shown in Fig. 6 and Table 3, temporal variations of rainfall δD and $\delta^{18}O$ at Chenqi are marked, ranging from -120.2 to -17.9‰ for δD and from -16.4 to 0‰ for $\delta^{18}O$. The δD and $\delta^{18}O$ responses amongst the depression wells are attenuated or damped but they are markedly different in this restricted area due to spatial heterogeneity of the karst aquifer (Table 3 and Fig 6). In terms of the temporal changes in δD and $\delta^{18}O$, values tended to become more negative in response to direct effects of rainwater recharge into the aquifer during storm events. Compared with isotope values at W1 and W5, groundwater at W3 and W4 is clearly receiving rainfall that has marked changes in isotope values evident in the variability in Fig 6 and the large range in Table 3. Groundwater at W5 is the most stable (Fig 6) and has the lowest range in Table 3 implying a limited influence of new recharge from rainfall. However, W1 is close to the catchment outlet and the high permeability of its lower aquifer inferred from the ERT survey may allow exchange with the subsurface flow leaving the catchment (Fig 3). The isotopic signatures of groundwater at W1 show intermediate isotopic values compared to the upper catchment (lower than the most stable water at W5 and higher than those at W3 and W4 where the direct rainfall influence is evident), suggesting that groundwater at W1 likely reflects mixing of flow paths from the upper depression.

However, at the different stages of the storm event response (e.g. the sharp rises and falls in water level before and after rainfall), the degree of “new” event water recharge from rainfall and “old” water release from previous storage amongst the four wells differed according to the δD values from the depression aquifer (Fig 7). Generally, recharge of new rainfall occurs in the early recession phase of the groundwater response, and the release of previously stored (old) water occurs later in the recession. The impact of infiltrating new water in the early recession can be distinguished from changes of the δD values before rainfall and in the early recession in Fig 7; for rainfall events No. 1 and 4, as the rainwater δD values are much more negative than those of the groundwater. The subsequent decline of the δD values in these depression wells indicates the ingress of isotopically depleted (newer) rainwater. However, for rainfall event No 3, as the rainwater δD is more enriched than groundwater, the rise of the δD values at these depression wells also indicates the impact of more enriched rainwater recharge.

In the later recession, the effects of recent recharge generally decline. Hence, the δD values of groundwater increase again for rainfall events No 2 and 4. This would be consistent with the release of older water into aquifer. As shown in Fig 7, changes of the δD values in the three events are evident for wells W3, W4 and W5, but the changes become less distinguishable for well W1 close to the catchment outlet (Fig 7). This also indicate that groundwater at the catchment outlet can be attributed by regional flow that endures a relatively high mixture of event new water with storage old water.

3.2 Hillslope-depression flow connectivity

Hillslope-depression flow connectivity can be identified from temporal variability in water table levels, temperatures and isotopic tracers at W4 located at the base of a steep hillslope and the hillslope spring (HS). Despite the marked response to rainfall events, the water level at W4 recesses much more slowly after rainfall ceases compared to the other wells (Fig 4). The slow recession in this interpreted high permeability area possibly arises from some additional water from upslope areas that continues to recharge the depression aquifer after rainfall ceases.

Water temperatures and isotopic values at W4 and the hillslope spring (HS) further provided evidence for hillslope contributions to the depression. Water temperatures at both sites show a similar pattern of the seasonal variations with air temperature and fluctuations with rainfall (see Fig 5), i.e. higher in the summer season and lower in the winter season. Water isotopic values at W4 are closest to these at the hillslope spring (HS), particularly, during the rainfall period (see the yellow for W4 and the green for HS in Fig 6 and mean values in Table 3). Additionally, in the winter season, water temperature at W4 is more attenuated and lags behind that of the hillslope spring, which indicate that the hillslope flow is faster than the depression groundwater flow at W4. In the summer season, the response of water temperature to rainfall at W4 is more marked that those of the hillslope spring, which indicate that the depression groundwater flow at W4 could receive hillslope flow as well as rainfall recharge.

3.3 Effect of vertical heterogeneity on hydrological functions

The ERT survey demonstrates strong vertical heterogeneity of the karst aquifer at each site (Fig 3). The δD values at various depths to groundwater table (the uncertainty bar in Fig 7) illustrates the effect of vertical heterogeneity on hydrological functions. For the four wells, the range of the vertical variation in δD is generally much higher for W1 and W3 in the central and outlet depression, than the wells of W4 and W5 at the upper depression. This is consistent with groundwater in the upper depression areas mixing more effectively in a vertical direction than groundwater in the center and catchment outlet.

The isotopic values prior to rainfall and at the early and late stages of the recession for rainfall event 4 (12 to 14 August 2017) in Fig 8 further demonstrate the control of vertical heterogeneity in aquifer structure on hydrological function. The event has a total rainfall of 36.8 mm and the rainfall δD value ranging between -109.8 and -74.8‰ with a mean of -90.7‰, with the most negative values coinciding with peak rainfall. The event-scale changes in the vertical distribution of the δD values are different for the four wells.

(1) ***W1:*** there is little vertical variation of the δD values before rainfall (Fig 8a(i), which indicates strong pre-event vertical mixing. Early in the recession when groundwater levels rapidly decline, the mean δD value declined from -60.5 to -61.6‰ (Fig 8a(i)), indicating some new water influence. Moreover, the flow paths of the new water ingress can be identified from the vertical variation of the δD values (see 13/8 line in Fig 8a(ii)), i.e. at the depths of 7-8m and below 18m where the δD values rapidly decline. These depths correspond to low resistivity regions indicative of high permeable layers (green in Fig 8a(iii)). Since the

temperature variation in Fig 5 and ERT image in Fig 8a(iii) suggest that the lower layer at W1 receives little rainfall recharge, the decline of the δD values seems most likely explained by exchange of groundwater in the high permeability depths with the regional flow (affected by new rainfall). Between the two higher permeability layers, water in the less permeability layer (yellow in Fig 8a(iii)) changes only little, indicating that flow exchange between the permeable and less permeable layers is weak.

Later in the recession, the δD value increases to -60.8‰, which is close to the pre-rainfall value. At this time, vertical variations on 14 August (Fig 8a(ii)) demonstrate that the δD value in the lower permeable layer (below 18m) recovers close to pre-event conditions. Surprisingly, the δD values in the upper less permeable layer (the depth of 7.5 m) become much less negative. This suggests that there may be release or displacement of older water, possibly attributable to antecedent storage from the upper less permeable layer (Fig 8a(iii)).

(2) ***W3:*** temporal variation of δD values over the three periods (Fig.8b(i)) is similar but more marked than that at W1. Vertical variation at W3 (Fig 8b(ii)) is very different over the three periods. Before the rainfall on 12 August, the δD values generally are less negative throughout the water column. The more negative values in the upper profile may reflect more recent depleted rainfall and increasingly older water with depth. This seems consistent with the decreasing permeability with depth at W3 implied by the less resistive upper profile and more resistive deeper layers (Fig 8b(iii)).

In the early recession on 13 August, δD values (Fig 8b(ii)) become more negative and almost uniform in vertical distribution. This implies that new water from recharge of rainwater rapidly mixes with older pre-event water in storage. In the later recession, groundwater isotope values recover indicating lessening influence of new water, though values do not recover to pre-rainfall levels. Meanwhile, groundwater in the upper aquifer (e.g. above 8m) still remains negative with continued new water influence. This suggests that the upper, more permeable (i.e. with lower resistivity) aquifer stores more new water during rainfall and releases this thereafter.

(3) ***W4:*** as shown in Fig.8c(i), the water level recession is slower than the other wells but the mean of the δD value declines greatly from -59‰ before rainfall to -67‰ in the early recession and then recovers to -65.9‰ in the later recession. The marked decline of δD is again consistent with substantial influence of event water ingress. Prior to rainfall when groundwater level is low (>4m in depth), the vertical distribution of the δD is nearly uniform (Fig 8c(ii)). In the early recession when water levels remain high, groundwater in the upper aquifer (above the depth of 3.5) tends to be more negative indicating event new water influence.

In the later recession, the δD values below 3.5m become a little more negative, whilst the upper aquifer remains the same. As W4 is located at the foot of a steep hillslope, it is likely that lateral flow from the hillslope contributes recharge since the ERT image suggests that this is a high permeability area strongly connected to the hillslope flow path (Fig 3 and Fig 8c(iii)).

(4) ***W5:*** The water level and isotopic response at W5 contrasts markedly to the other wells, i.e. a transient fluctuation of water level and abrupt change in δD (Fig 8d(i)). The

unresponsive groundwater likely reflects that the well is located in an impervious (high resistivity) area (Fig 8d(iii)). After the water level decline, groundwater has a limited decrease in δD (from -58 to -58.4‰) in the early post-event period, and continuous decrease (to -59.6‰) later. The continuous decease of δD values indicates a longer memory of the much less permeability aquifer to the limited recharge.

Before rainfall, the vertical values of δD are highly varied; water in the upper layer has less negative values of δD, whilst waters at depths of 7.4m and below 8m have more negative values of δD (Fig 8d(ii)). The much older water in the upper layer suggests strong evaporative effect in the non-rainfall period since the top soils and the upper permeability rock layer are thin (Fig 8d(iii)) and thus evaporative effect is strong. Marked changes of the δD values in the lower depths (e.g. below 7.4m) reflects that there are still some permeable fractures, in which new water could be arrival. After the end of the brief water table response, the vertical δD values (13 August in Fig 8d(ii)) in the lower layer (e.g. below 7.4m) are more negative than the upper layer. This would imply that after a short response to rainfall (Fig 8d(i)), event "new" water in the upper layer rapidly mixes with the surrounding "old" water, but "new water" still ingresses into the lower depths. In the later post-event period, the relatively uniform vertical values of δD (14 August in Fig 8d(ii)) show recharged event water mixing in the whole profile.

4 Discussion and conclusions

4.1 Discussion

4.1.1 Conceptualizing hydrological functions in cockpit karst catchment

Variation in hydrological functions (rainfall recharge, horizontal and vertical flow exchange at sites and hillslope-depression connectivity) in the heterogenous subsurface of our cockpit karst catchment can be summarized as in Fig 9. Fast and frequent rainwater recharge I_f into the epikarst zone on the hillslope (HS) and permeable depression (e.g. W3 and W4) leads to local flow being "active" and young, whilst infrequent rainwater recharge into the less permeable depression (e.g. W1 and W5) leads to local flow being less active or inactive and "old". For the hillslope-depression-outlet connectivity, the mean isotopic value at outlet (δD) is between relatively "new" water from fast flows in HS and high permeability depression areas (W3 and W4) (δD_f) and "old" water from slow flows in low permeability depression areas (W1 and W5) (δD_s). Thus, outlet water (Q and δD) can be viewed as a mixture of hillslope (Q_f and δD_f) and depression flow (Q_s and δD_s) at various sites.

Fig 8 shows that temporal change in hydrological functions is closely linked to vertical heterogeneity with different composition of the active, less active and inactive areas. The structure of the vertical profile can be generalized as Fig 9 and classified into two types: (a) profiles consisting of two different permeability layers, e.g. a high permeability layer confined by a lower permeability layer at W1 and a high permeability layer with limited thickness perched on a less permeability layer at W5. (b) profiles comprising one layer but their permeability decreasing with depth, e.g. at W3 and W4. Here, the profile flow function can be still illustrated by exchange of fast and slow flow reservoirs (Fig 9) but the relative contribution of fast and slow flow reservoirs is a function of depth h, i.e. $Q\delta D(h) = Q_f\ \delta D_f(h) + Q_s\ \delta D_s(h)$, in where flows and isotopic values in each reservoir are influenced by rainfall recharge I_f and water exchange between fast and slow reservoirs Q_E=K_E(h) (WT_f -WT_s) (WT_f and WT_s represent water table in the fast and slow reservoirs, respectively, and K_E is exchange coefficient).

Such depth variability of hydrological function can be used to explain the hydrological response of the observation wells (Fig 9). The profile depth h at W1 and W5 can be divided into two homogenous layers ($h1$ and $h2$). At W1, we can hypothesize that recharge of the fast flow reservoir (I_f) is negligible due to the upper confining layer. The fast flow Q_f can be highly connected with the regional flow but has limited exchange with the slow flow reservoir Q_s i.e. Q_E is small, evidenced by little change of the δD value in the less permeable layer for W1 in Fig 8a(i). At W5, groundwater in the profile id dominated by the slow reservoir Q_s in the lower layer (h2>>h1). Before rainfall, when the water level WT_s is low, limited perched water Q_f in the upper layer ingresses into the slow reservoir (Q_E can be neglected). During rainfall when the upper water table WT_f rises higher than the low water table WT_s, pressure drives new event water Q_f into the slow reservoir in a short time (Q_E is slight and transient). After rainfall when a short pulse of water table variation ends (WT_f<= WT_s), the pressured new water in the slow reservoir Q_s is slowly released.

The hydrological functions in the profiles W3 and W4 can be still conceptualized into the fast and slow flow reservoirs in which fast flow contribution (Q_f) to the whole profile flow gradually reduces with depth whilst the slow flow contribution (Q_s) increases. As the profile is highly permeable and unconfined, direct recharge into the fast reservoir (I_f) and new event water quickly mixes with pre-event water in the vertical direction under WT_f>=WT_s during rainfall (large Q_E). In the later recession when water table is low and WT_f<=WT_s, the older water in the slow flow reservoir is mostly released from the lower layers (Fig.9b), i.e. less negative $\delta D_s(h)$ and larger Q_s in $Q\delta D(h) = Q_f\,\delta D_f(h) + Q_s\,\delta D_s(h)$. The unconfined aquifer at W4 is similar to W3 but the aquifer at W4 receives direct recharge (I_f) and inputs from hillslope flow (Q_h) during events when water levels are high, then quickly infiltrates into the low slow reservoir (large Q_E). After rainfall, the upper fast reservoir retains a water level higher than the slow reservoir (WT_f>=WT_s) since the hillslope flow (Q_h) continually inputs into the aquifer (evidenced by more negative of the δD values in Fig 7c(ii)).

In any specific landscape unit (e.g. depression), outlet flow Q comes from fast and slow flow composition at various sites, i.e. $Q = \sum_1^n Q_f + \sum_1^n Q_s$, and $Q\delta D = \sum_1^n Q_f \delta D_f + \sum_1^n Q_s \delta D_s$, where n is the total number of the sites. Meanwhile, in each reservoir, the discharge ($\sum_1^n Q_f$ or $\sum_1^n Q_s$) and the mass ($\sum_1^n Q_f \delta D_f$ or $\sum_1^n Q_s \delta D_s$) are influenced by rainfall recharge I_f and flow exchange Q_E. More specifically, considering vertical heterogeneity at the sites, outlet flows Q and mass $Q\delta D$ can be expressed by: $\sum_1^n \sum_1^{n1} Q_f + \sum_1^n \sum_1^{n2} Q_s$ and $\sum_1^n \sum_1^{n1} Q_f\, \delta D_f + \sum_1^n \sum_1^{n2} Q_s\, \delta D_s$, respectively, where n1 and n2 are the respective number of permeable and less permeable layers in a profile.

4.1.2 Benefits of an integrated approach

Karst aquifers have distinct hydraulic structures and behaviors and therefore require specific investigation methods (Goldscheider and Drew 2007). Capturing the hydrological functions requires hydrometric observations and tracer sampling at sub-hourly intervals as shown in our study. Current techniques that deploy loggers with the capacity to monitor in real-time and the capability to transfer data remotely are particularly useful (Luhmann et al., 2015). In general, monitoring water level data is easy and cheap and it reflects the relatively strong control of rainfall frequency on hydrograph shape. Nevertheless, it has limited value in interpreting karst aquifer structures (Jeannin and Sauter, 1998) and identifying the contributions of event and pre-event water. The non-conservative nature of water temperature facilitates insights into conduit size, and the damping and retardation in porous media via an analysis of input and output thermographs (Covington et al., 2011, 2012; Luhmann et al., 2012; Birk et al., 2014; Luhmann et al., 2015). However, reliable identification of the hydrological functions from input and output thermographs need integrate information on heat exchange within karst conduits that may introduce a retardation in the residence times (Luhmann et al., 2015). Comparison of the temporary variation of isotopic values in rainfall with the observed variability in karst spring waters allows not only quantification of mixing processes in discharge as shown in our study, but also to quantify transit time distributions (Hu et al., 2015) and determine groundwater ages.

Selecting representative sites is challenging and important in capturing the large-scale hydrological functions in the karst catchment due to strong heterogeneity, hydraulic discontinuity and anisotropy. Traditionally, tracing and hydrometric observations have been mostly undertaken in the conduit network to study the rapid flow (Goldscheider et al. 2008) and at outlet springs for the overall characterization of karst systems (Kovacs and Perrochet, 2008). However, fractured rocks in the karst critical zone have the permeability ranging over several orders of magnitude. Even at small spatial scales (e.g. the four wells in our study catchment), there is relatively less active subsurface flow in the high permeability zones, and relatively active subsurface flow in the less permeable zones. Additionally, our analyzed results of new event water recharge and the degree of mixing with pre-event old water indicates that water samples at representative depths to characterize subsurface inflows to wells are necessary for assessing different flow paths in the karst and temporal changes in their hydrological dynamics.

A key contribution of this study was to show how geophysical techniques like ERT surveys can help identifying structural differences which can be incorporated in designing targeted monitoring networks. ERT images combined with tracer characteristics of subsurface water and the associated mixing processes identify which depths/sites in the catchment are representative for monitoring in order to reliably quantify fast and slow flows. As shown in Fig 8, water sampling at permeable layers/sites during rainfall events are required for capturing variability of the hydrological functions in the karst catchment. If the permeability varies with depth, water sampling at various depths are particularly important for quantifying the depth-dependent variability of the hydrological function.

Moreover, ERT images combined with details observations provide insights into how to conceptualize complex karst systems for lumped and distributed modeling. ERT images provide high-resolution visualization of the subsurface, and the relationship between these images and parameters affecting flow and transport (Hubbard et al., 1999). The spatially distributed information from geophysics and isotopic characterisation of subsurface water and the associated mixing processes facilitate tracing water flow sources (e.g. rainfall recharge and exchange between high and low permeable sites/layers). This understanding can inform hydrological model structures at different scales (e.g. as conceptualized fast and slow flow reservoirs) and their hydrological connectivity (e.g. hillslope-depression-outlet). The inferred hydrologic characteristics can be then used either independently or combined with direct hydrologic observations to constrain hydrologic properties and reduce uncertainty in hydrological models (Hinnell et al., 2010).

4.2 Conclusions

Understanding the function of the water cycle is a key issue for critical zone science since water is a unifying theme for understanding complex environmental systems (Lin, 2010). Nevertheless, it is a significant challenge to identify active subsurface processes that determine water flows and travel times. In this study, geophysical, hydrometric and tracer tools are used to characterize the hydrological function of the cockpit karst critical zone in the small catchment of Chenqi, Guizhou province, China. The ERT surveys (Fig 2) identified structural features that likely control aquifer permeability and the heterogeneity in observed hydrodynamic response. Hydrometric observations and using water temperatures (Figs 2 and 3) as a tracer clearly identified rainfall recharge and flow recession induced by new rainwater recharge and the constraints of aquifer permeability. Stable water isotopes (δD and $\delta^{18}O$) (Fig 5) largely corroborated geophysical, hydrometric and thermal data and provided detail qualitative insight into event water recharge into, and pre-event storage release from, the heterogeneous aquifer. In particular, this information can help identify flow paths of new event water recharging through high permeability zones in both horizontal and vertical directions in the catchment.

The study illustrated that even in a highly heterogeneous catchment, hydrological functions can be conceptualized simply into fast and slow flow reservoirs. Nevertheless, using such a dual flow system in simulation of hydrological processes should be based on detail observations at representative sites within a catchment. Particularly, since hydrological functions can vary with depth, observations and water sampling from various permeability layers are extremely important.

Acknowledgments

This research was supported by The UK-China Critical Zone Observatory (CZO) Programme (41571130071), the National Natural Scientific Foundation of China (41571020), National 973 Program of China (2015CB452701), the National Key Research and development Program of China (2016YFC0502602), the Fundamental Research Funds for the Central Universities (2016B04814) and the UK Natural Environment Research Council (NE/N007425/1 & NE/N007409/1). We thank the editor and the two anonymous reviewers for their constructive comments on the earlier manuscript, which lead to an improvement of the paper.

REFERENCES

Anderson MP. 2005. Heat as a ground water tracer. Ground Water 43 (6): 951–968 DOI: 10.1111/j.1745-6584.2005.00052.x

Aquilina L, Ladouche B, Dörfliger N. 2006. Water storage and transfer in the epikarst of karstic systems during high flow periods. Journal of Hydrology 327 (3–4): 472–485 DOI: 10.1016/j.jhydrol.2005.11.054

Barberá JA, Andreo B. 2012. Functioning of a karst aquifer from S Spain under highly variable climate conditions, deduced from hydrochemical records. Environmental Earth Sciences 65 (8): 2337–2349 DOI: 10.1007/s12665-011-1382-4

Batiot C, Emblanch C, Blavoux B. 2003. Total Organic Carbon (TOC) and magnesium (Mg2+): two complementary tracers of residence time in karstic systems. Comptes Rendus Geoscience 335 (2): 205–214 DOI: 10.1016/S1361-0713(03)00027-0

Becker MW, Georgian T, Ambrose H, Siniscalchi J, Fredrick K. 2004. Estimating flow and flux of ground water discharge using water temperature and velocity. Journal of Hydrology 296 (1–4): 221–233 DOI: 10.1016/j.jhydrol.2004.03.025

Binley, A, 2015, Tools and Techniques: DC Electrical Methods, In: Treatise on Geophysics, 2nd Edition, G Schubert (Ed.), Elsevier., Vol. 11, 233-259, doi:10.1016/B978-0-444-53802-4.00192-5.

Binley A, Hubbard SS, Huisman JA, Revil A, Robinson DA, Singha K, Slater LD. 2015. The emergence of hydrogeophysics for improved understanding of subsurface processes over multiple scales, Water Resources Research, 51(6), 3837-3866, DOI:10.1002/2015WR017016

Biswas H, Sena DR, Kumar G, Lakaria BL, Raizada A, Kumar S, Mishra PK. 2017. Effect of water storage structures on groundwater recharge in India. Groundwater for Sustainable Development 4: 49–56 DOI: 10.1016/j.gsd.2017.01.002

Birk S, Wagner T, Mayaud C. 2014. Threshold behavior of karst aquifers: The example of the Lurbach karst system (Austria). Environmental Earth Sciences 72 (5): 1349–1356 DOI: 10.1007/s12665-014-3122-z

Carrière SD, Chalikakis K, Sénéchal G, Danquigny C, Emblanch C. 2013. Combining Electrical Resistivity Tomography and Ground Penetrating Radar to study geological structuring of karst Unsaturated Zone. Journal of Applied Geophysics 94: 31–41 DOI: 10.1016/j.jappgeo.2013.03.014

Chalikakis K, Plagnes V, Guerin R, Valois R, Bosch FP. 2011. Contribution of geophysical methods to karst-system exploration: An overview. Hydrogeology Journal 19 (6): 1169–1180 DOI: 10.1007/s10040-011-0746-x

Coplen TB. 1994. Reporting of stable hydrogen, carbon, and oxygen isotopic abundances (Technical Report). Pure and Applied Chemistry 66 (2): 273–276 DOI: 10.1351/pac199466020273.

Covington MD, Luhmann AJ, Gabrovek F, Saar MO, Wicks CM. 2011. Mechanisms of heat exchange between water and rock in karst conduits. Water Resources Research 47 (10) DOI: 10.1029/2011WR010683.

Covington MD, Luhmann AJ, Wicks CM, Saar MO. 2012. Process length scales and longitudinal damping in karst conduits. Journal of Geophysical Research: Earth Surface 117 (1) DOI: 10.1029/2011JF002212.

Emblanch C, Zuppi GM, Mudry J, Blavoux B, Batiot C. 2003. Carbon 13 of TDIC to quantify the role of the unsaturated zone: The example of the Vaucluse karst systems (Southeastern France). Journal of Hydrology 279 (1–4): 262–274 DOI: 10.1016/S0022-1694(03)00180-X

Fan J, Oestergaard KT, Guyot A, Lockington DA. 2014. Estimating groundwater recharge and evapotranspiration from water table fluctuations under three vegetation covers in a coastal sandy aquifer of subtropical Australia. Journal of Hydrology 519 (PA): 1120–1129 DOI: 10.1016/j.jhydrol.2014.08.039

Field MS. 1993. Karst Hydrology and Chemical Contamination. Journal of Environmental Systems 22 (1): 1–26 DOI: 10.2190/X7MV-C93E-66GK-BFH7

Ford D, Williams P. 2013. Karst Hydrogeology and Geomorphology. DOI: 10.1002/9781118684986

Goldscheider N, Drew D. 2007. Methods in Karst Hydrogeology. Taylor & Francis Group, Leiden, NL.

Hartmann A, Goldscheider N, Wagener T, Lange J, Weiler M. 2014. Karst water resources in a changing world: Approaches, of hydrological modeling. Review of Geophysics (1): 1–25 DOI: 10.1002/2013RG000443

Healy RW, Cook PG. 2002. Using groundwater levels to estimate recharge. Hydrogeology Journal 10 (1): 91–109 DOI: 10.1007/s10040-001-0178-0

Hinnell AC, Ferr TPA, Vrugt JA, Huisman JA, Moysey S, Rings J, Kowalsky MB. 2010. Improved extraction of hydrologic information from geophysical data through coupled hydrogeophysical inversion. Water Resources Research 46 (4) DOI: 10.1029/2008WR007060.

Hu K, Chen H, Nie Y, Wang K. 2015. Seasonal recharge and mean residence times of soil and epikarst water in a small karst catchment of southwest China. Scientific Reports 5 DOI: 10.1038/srep10215.

Hubbard SS, Rubin Y, Majer E. 1999. Spatial correlation structure estimation using geophysical and hydrogeological data. Water Resources Research 35 (6): 1809–1825 DOI: 10.1029/1999WR900040.

Hyman JD, Painter SL, Viswanathan H, Makedonska N, Karra S. 2015. Influence of injection mode on transport properties in kilometer-scale three-dimensional discrete fracture networks. Water Resources Research 51 (9): 7289–7308 DOI: 10.1002/2015WR017151.

Irvine DJ, Cranswick RH, Simmons CT, Shanafield MA, Lautz LK. 2015. The effect of streambed heterogeneity on groundwater-surface water exchange fluxes inferred from temperature time series. Water Resources Research 51 (1): 198–212 DOI: 10.1002/2014WR015769

Jeannin PY, Sauter M. 1998. Analysis of karst hydrodynamic behaviour using global approaches: A review. Bull/d'Hydrogéologie 16: 31–48.

620 Jiang G, Guo F, Wu J, Li H, Sun H. 2008. The threshold value of epikarst runoff in forest karst mountain area. Environmental Geology 55 (1): 87–93 DOI: 10.1007/s00254-007-0967-4.

623 Kovács A, Sauter M. 2007. Modelling karst hydrodynamics. In: Goldscheider N, Drew D (eds) Methods in karst hydrogeology, vol 26. International Contribution to Hydrogeology, Heise, Hanover, Germany, pp 201–220

626 Lee LJE, Lawrence DSL, Price M. 2006. Analysis of water-level response to rainfall and implications for recharge pathways in the Chalk aquifer, SE England. Journal of Hydrology 330 (3–4): 604–620 DOI: 10.1016/j.jhydrol.2006.04.025

629 Lin H. 2010. Earth's Critical Zone and hydropedology: concepts, characteristics, and advances. Hydrol. Earth Syst. Sci., 14, 25–45

631 Long JCS, Remer JS, Wilson CR, Witherspoon PA. 1982. Porous media equivalents for networks of discontinuous fractures. Water Resources Research 18 (3): 645–658 DOI: 10.1029/WR018i003p00645.

634 Long AJ, Putnam LD. 2004. Linear model describing three components of flow in karst aquifers using 18O data. Journal of Hydrology 296 (1–4): 254–270 DOI: 10.1016/j.jhydrol.2004.03.023

637 Lowry CS, Walker JF, Hunt RJ, Anderson MP. 2007. Identifying spatial variability of groundwater discharge in a wetland stream using a distributed temperature sensor. Water Resources Research 43 (10) DOI: 10.1029/2007WR006145

Luhmann AJ, Covington MD, Alexander SC, Chai SY, Schwartz BF, Groten JT, Alexander EC. 2012. Comparing conservative and nonconservative tracers in karst and using them to estimate flow path geometry. Journal of Hydrology 448–449: 201–211 DOI: 10.1016/j.jhydrol.2012.04.044.

Luhmann AJ, Covington MD, Myre JM, Perne M, Jones SW, Alexander EC, Saar MO. 2015. Thermal damping and retardation in karst conduits. Hydrology and Earth System Sciences 19 (1): 137–157 DOI: 10.5194/hess-19-137-2015.

Martínez-Moreno FJ, Galindo-Zaldívar J, Pedrera A, Teixido T, Ruano P, Peña JA, González-Castillo L, Ruiz-Constán A, López-Chicano M, Martín-Rosales W. 2014. Integrated geophysical methods for studying the karst system of Gruta de las Maravillas (Aracena, Southwest Spain). Journal of Applied Geophysics 107: 149–162 DOI: 10.1016/j.jappgeo.2014.05.021

Mudarra M, Andreo B, Marín AI, Vadillo I, Barberá JA. 2014. Combined use of natural and artificial tracers to determine the hydrogeological functioning of a karst aquifer: the Villanueva del Rosario system (Andalusia, southern Spain). Hydrogeology Journal 22 (5): 1027–1039 DOI: 10.1007/s10040-014-1117-1

Mudarra M, Andreo B. 2011. Relative importance of the saturated and the unsaturated zones in the hydrogeological functioning of karst aquifers: The case of Alta Cadena (Southern Spain). Journal of Hydrology 397 (3–4): 263–280 DOI: 10.1016/j.jhydrol.2010.12.005

Niswonger RG, Prudic DE, Pohll G, Constantz J. 2005. Incorporating seepage losses into the unsteady streamflow equations for simulating intermittent flow along mountain front streams. Water Resources Research 41 (6): 1–16 DOI: 10.1029/2004WR003677.

Perrin J, Jeannin PY, Zwahlen F. 2003. Epikarst storage in a karst aquifer: A conceptual model based on isotopic data, Milandre test site, Switzerland. Journal of Hydrology 279 (1–4): 106–124 DOI: 10.1016/S0022-1694(03)00171-9.

Plummer LN, Busenberg E, McConnell JB, Drenkard S, Schlosser P, Michel RL. 1998. Flow of river water into a Karstic limestone aquifer. 1. Tracing the young fraction in groundwater mixtures in the Upper Floridan Aquifer near Valdosta, Georgia. Applied Geochemistry 13 (8): 995–1015 DOI: 10.1016/S0883-2927(98)00031-6

Rau GC, Andersen MS, McCallum AM, Acworth RI. 2010. Analytical methods that use natural heat as a tracer to quantify surface water-groundwater exchange, evaluated using field temperature records. Hydrogeology Journal 18 (5): 1093–1110 DOI: 10.1007/s10040-010-0586-0

Rau GC, Andersen MS, McCallum AM, Roshan H, Acworth RI. 2014. Heat as a tracer to quantify water flow in near-surface sediments. Earth-Science Reviews 129: 40–58 DOI: 10.1016/j.earscirev.2013.10.015

Sophocleous M. 2002. Interactions between groundwater and surface water: The state of the science. Hydrogeology Journal 10 (1): 52–67 DOI: 10.1007/s10040-001-0170-8

Sophocleous MA. 1991. Combining the soilwater balance and water-level fluctuation methods to estimate natural groundwater recharge: Practical aspects. Journal of Hydrology 124 (3–4): 229–241 DOI: 10.1016/0022-1694(91)90016-B

Soulsby C, Bradford J, Dick J, McNamara JP, Geris J, Lessels J, Blumstock M, Tetzlaff D. 2016. Using geophysical surveys to test tracer-based storage estimates in headwater catchments. Hydrological Processes 30 (23): 4434–4445 DOI: 10.1002/hyp.10889

Sprenger M, Tetzlaff D, Soulsby C. 2017. Soil water stable isotopes reveal evaporation dynamics at the soil-plant-atmosphere interface of the critical zone. Hydrology and Earth System Sciences 21 (7): 3839–3856 DOI: 10.5194/hess-21-3839-2017

Sprenger M. Tetzlaff D, Buttle JM, Snelgrove J, Laudon H, Mitchell C, Weiler M, Soulsby C. 2018. Measuring and modelling stable isotopes of mobile and bulk soil water. Vadose Zone Journal. DOI: 10.2136/vzj2017.08.0149.

Sun Z, Ma R, Wang Y, Ma T, Liu Y. 2016. Using isotopic, hydrogeochemical-tracer and temperature data to characterize recharge and flow paths in a complex karst groundwater flow system in northern China. Hydrogeology Journal 24 (6): 1393–1412 DOI: 10.1007/s10040-016-1390-2

Winter TC. 1999. Relation of streams, lakes, and wetlands to groundwater flow systems. Hydrogeology Journal 7 (1): 28–45 DOI: 10.1007/s100400050178

Xie Z, Yuan X. 2010. Prediction of water table under stream-aquifer interactions over an arid region. Hydrological Processes 24 (2): 160–169 DOI: 10.1002/hyp.7434

Williams PW. 1983. The role of the subcutaneous zone in karst hydrology. Journal of Hydrology 61 (1–3): 45–67 DOI: 10.1016/0022-1694(83)90234-2.

Worthington SRH, Jeannin P-Y, Alexander EC, Davies GJ, Schindel GM. 2017. Contrasting definitions for the term 'karst aquifer'. Hydrogeology Journal 25 (5): 1237–1240 DOI: 10.1007/s10040-017-1628-7.

Zhang Z, Chen X, Chen X, Shi P. 2013. Quantifying time lag of epikarst-spring hydrograph response to rainfall using correlation and spectral analyses. Hydrogeology Journal 21 (7): 1619–1631 DOI: 10.1007/s10040-013-1041-9.

Zhang Z, Chen X, Soulsby C. 2017. Catchment-scale conceptual modelling of water and solute transport in the dual flow system of the karst critical zone. Hydrological Processes 31 (19): 3421–3436 DOI: 10.1002/hyp.11268

Table 1 Statistical summary of water level and flow discharge

	Water Level (m)				Flow discharge (m^3/s)	
	W1	W3	W4	W5	Hillslope	Outlet
Min	1267.4	1272.6	1280.0	1276.4	0	0
Max	1275.9	1279.9	1285.2	1284.0	1.4×10^{-3}	0.15
Range	8.5	7.3	5.2	7.6	1.4×10^{-3}	0.15
Mean	1273.6	1275.9	1281.8	1278.9	8.5×10^{-5}	4.7×10^{-3}
Cv	0.03	0.21	0.61	0.07	1.73	2.83

Table 2 Statistical summary of air and water temperature

	Air	W1	W3	W4	W5	Hillslope	Outlet
T_{min} ℃	0	17.2	16.4	16.1	16.8	8.8	14.1
T_{max} ℃	35.6	17.5	22	19.6	17.5	21.1	21.3
Range	35.6	0.3	5.6	3.5	0.7	12.3	7.2
T_{mean} ℃	16.8	17.3	17.9	17.3	17.1	16.8	17.1
Cv	0.421	0.004	0.026	0.036	0.012	0.16	0.08

Table 3 Statistical summary of isotope data for rainfall, hillslope spring (HS), catchment outlet and depression wells

Obs	Period	δD (‰)					$\delta^{18}O$ (‰)				
		Max	Min	Range	Cv	Mean	Max	Min	Range	Cv	Mean
Rainfall	12/6~13/8	-17.9	-120.2	-102.3	-0.30	-73.2	0	-16.4	-16.4	-0.29	-9.9
outlet	12/6~14/8	-46.9	-73.1	-26.2	-0.06	-61.9	-5.1	-10.6	-5.5	-0.09	-8.7
HS	12/6~14/8	-51.8	-77	-25.2	-0.04	-64.3	-5.9	-10.8	-4.9	-0.06	-9.3
W1	6/7~20/8	-50.7	-65.7	-15	-0.03	-60.8	-6.3	-9.6	-3.3	-0.05	-8.7
W3	6/7~20/8	-56.1	-73.6	-17.5	-0.06	-62.4	-7.4	-10	-2.6	-0.06	-8.7
W4	6/7~20/8	-55	-70.2	-15.2	-0.07	-62.5	-7.9	-10.1	-2.2	-0.07	-8.9
W5	6/7~20/8	-55.7	-67.5	-11.8	-0.03	-58.7	-7.9	-10.1	-2.2	-0.04	-8.5

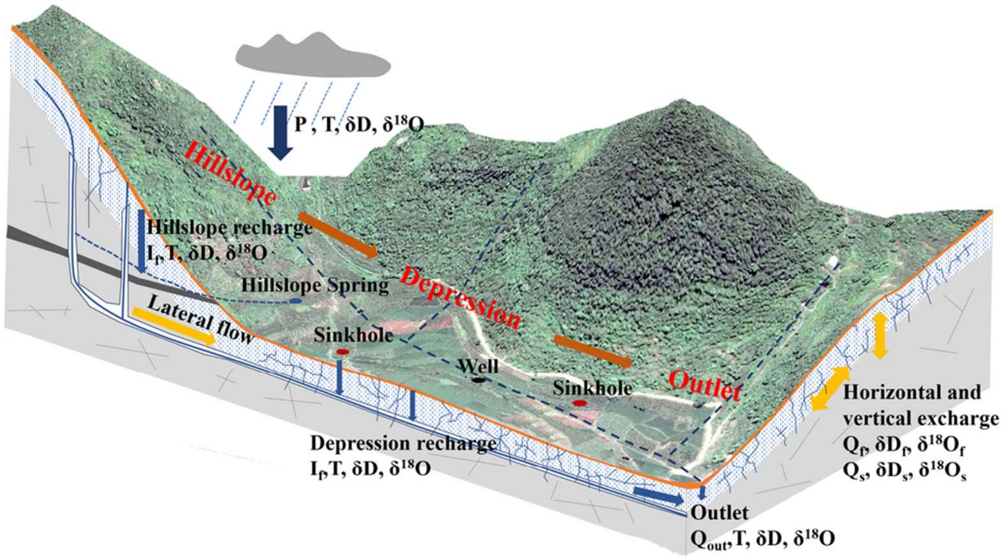

Figure 1 Sketch map of karst hydrological processes.

43x24mm (600 x 600 DPI)

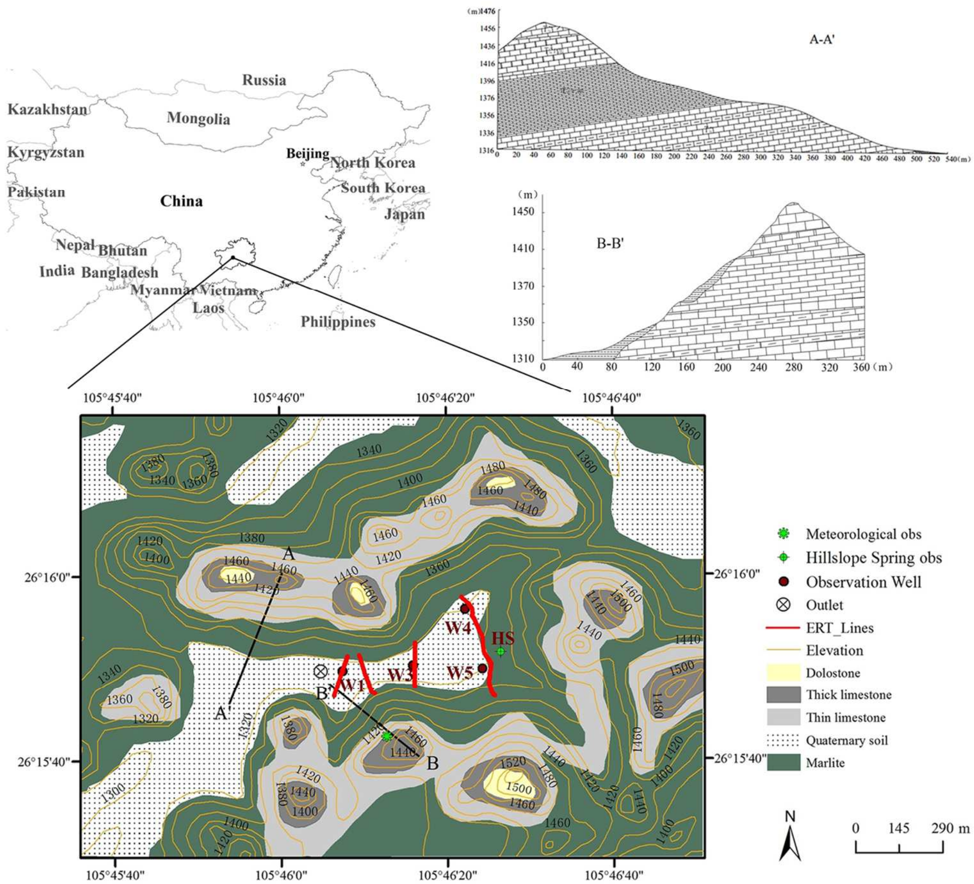

Figure 2 Map of geomorphology and hydrological monitoring locations in the Chenqi catchment.

59x53mm (600 x 600 DPI)

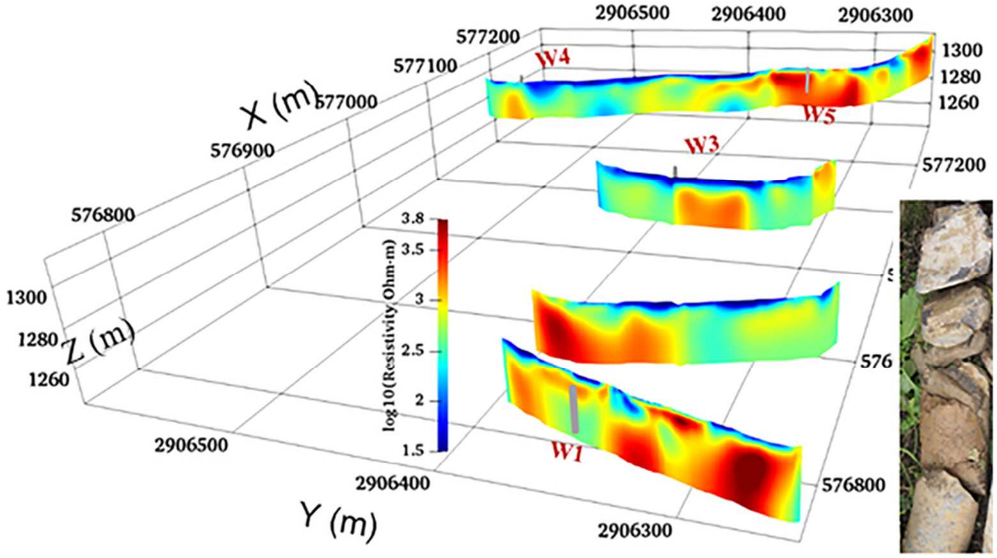

Figure 3 ERT image in the study depression corresponding to the survey profiles in Fig 1.

37x21mm (600 x 600 DPI)

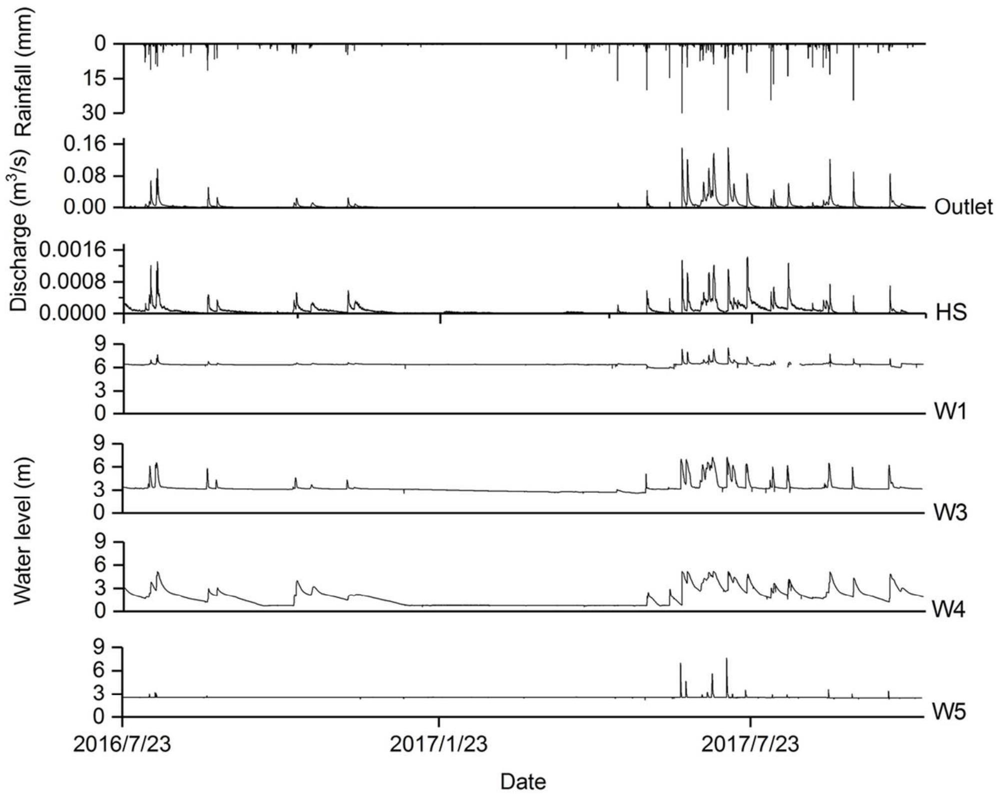

Figure 4 Variations of flow discharge for hillslope spring (HS) and catchment outlet and water levels at depression wells (W1, W3, W4 and W5).

52x41mm (600 x 600 DPI)

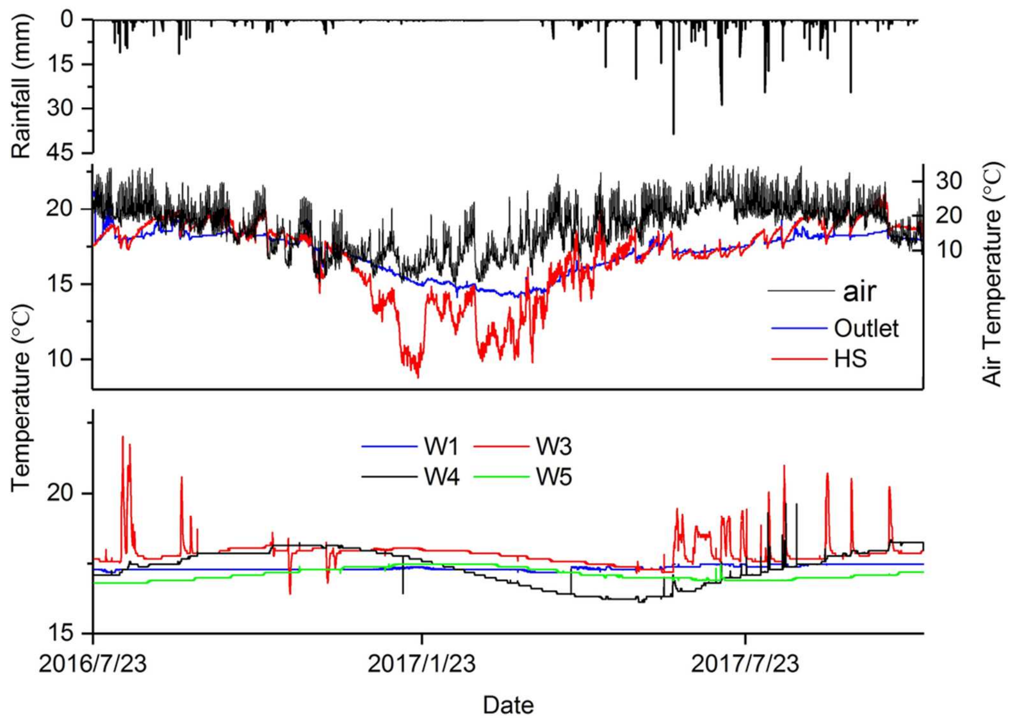

Figure 5 Variations of air temperature and water temperatures for hillslope spring (HS), outlet discharge and depression wells (W1, W3, W4 and W5).

46x33mm (600 x 600 DPI)

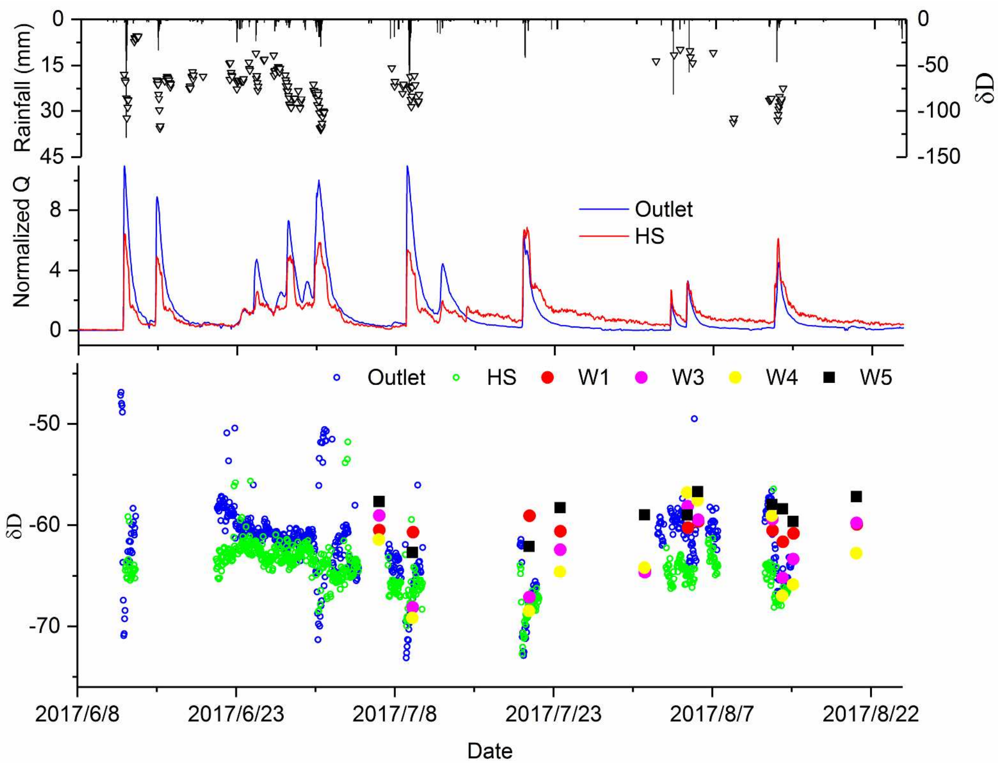

Figure 6 Variation of the δD values for rainfall, hillslope spring (HS), catchment outlet and depression wells.

148x113mm (600 x 600 DPI)

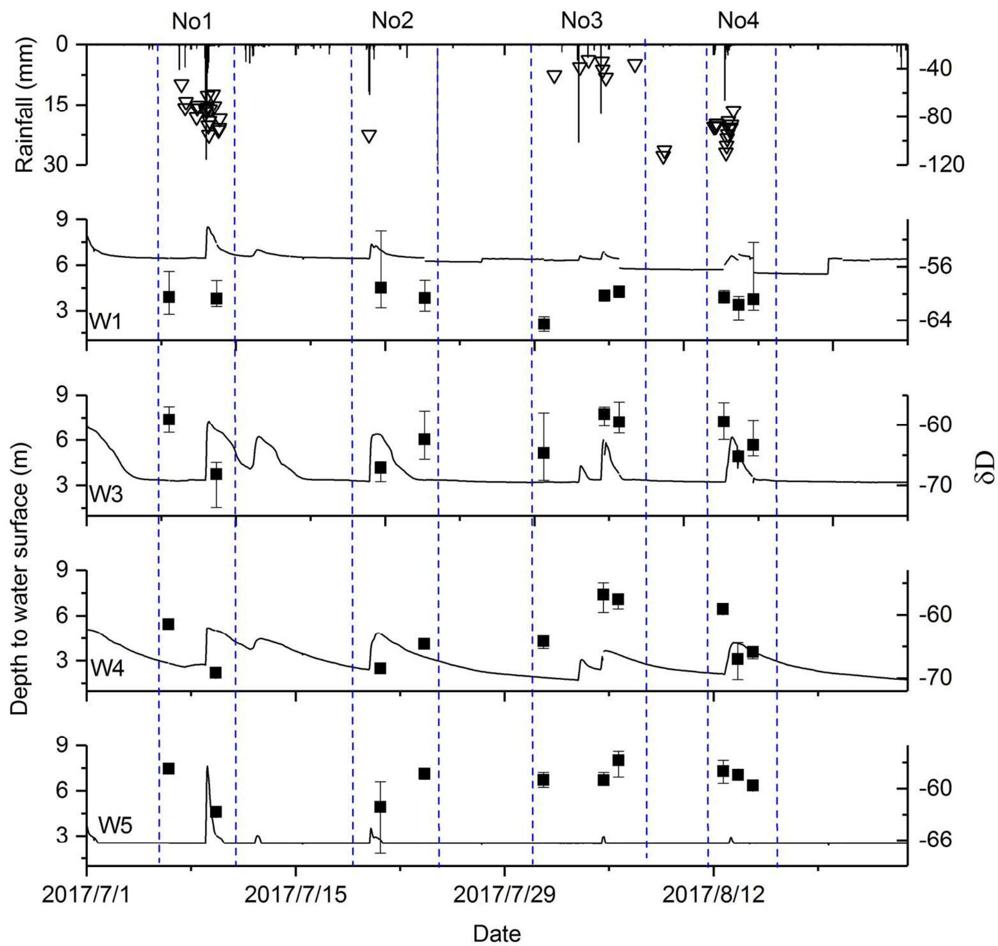

Figure 7 Variability of the δD values for depression wells (the bar represents range of δD values along various depths to water surface; black block represents its mean value; solid line represents depth to water table).

85x80mm (600 x 600 DPI)

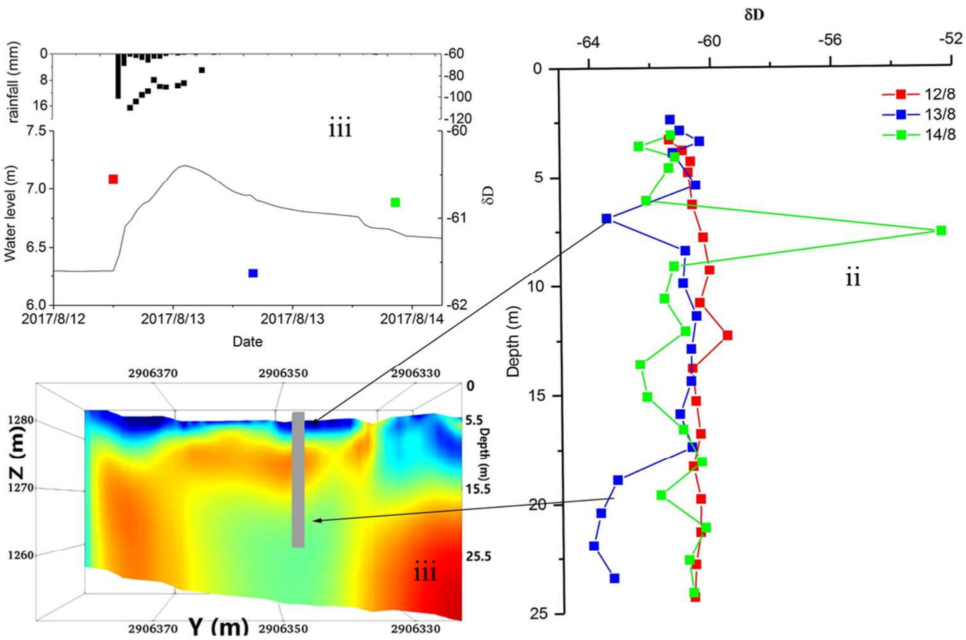

(a)

54x35mm (600 x 600 DPI)

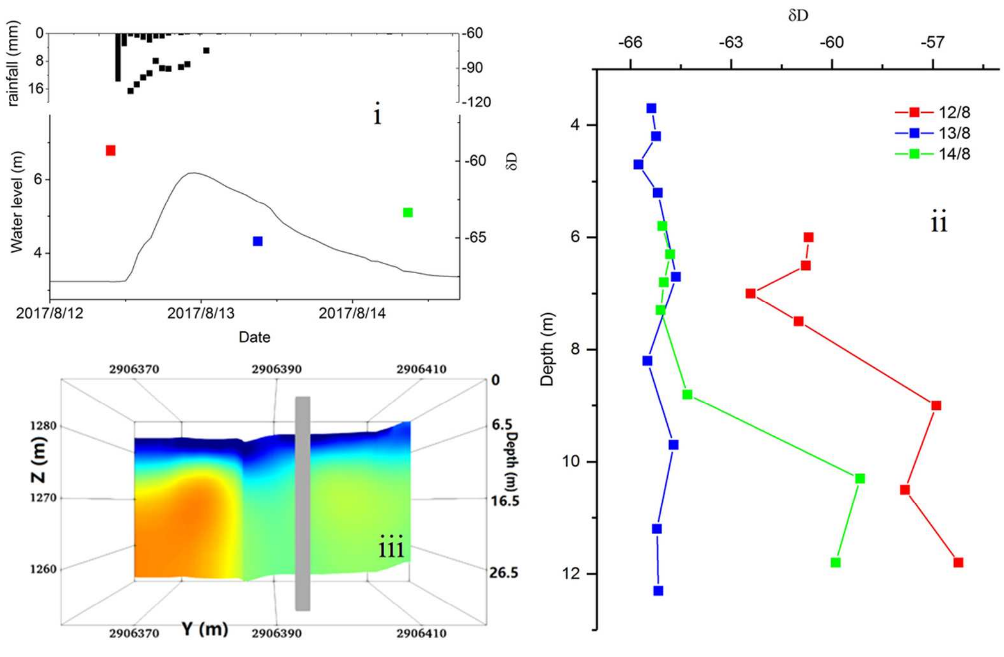

(b)

52x36mm (600 x 600 DPI)

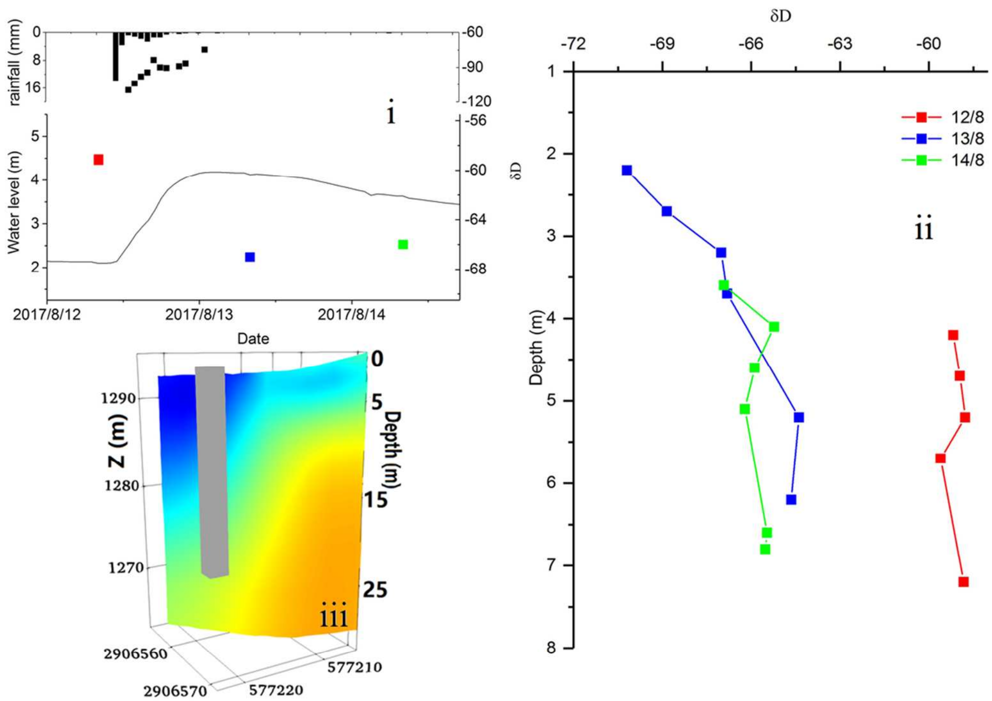

(c)

51x39mm (600 x 600 DPI)

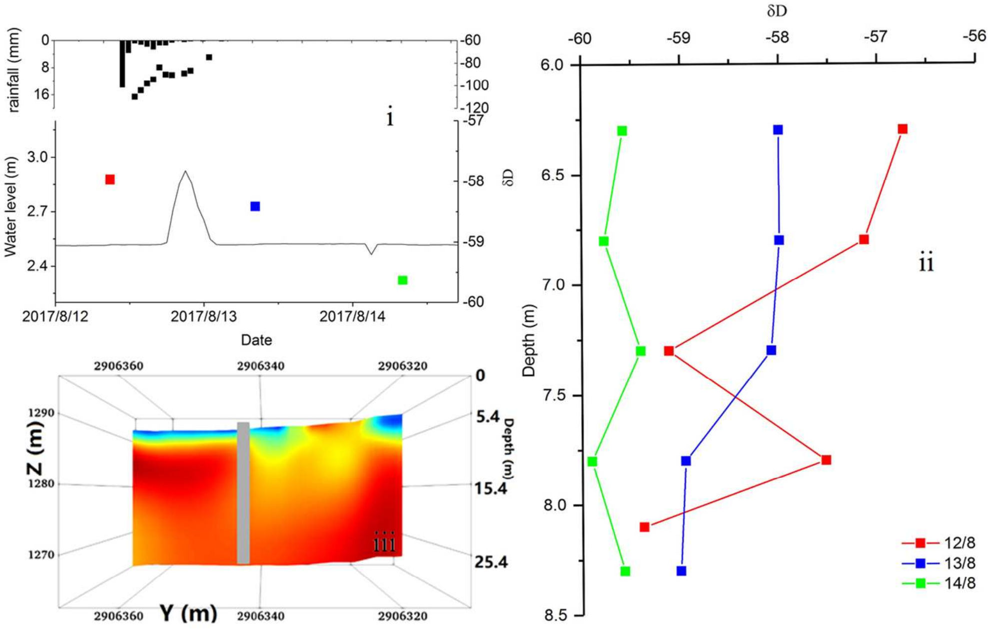

(d)

Figure 8 Variability of rainfall, water level and δD values (i), vertical distribution of groundwater δD values (ii) and ERT image (iii) of W1 (a), W3 (b), W4(c) and W5(d). The colour dots in the (i) plots are the mean δD value of different depths.

58x40mm (600 x 600 DPI)

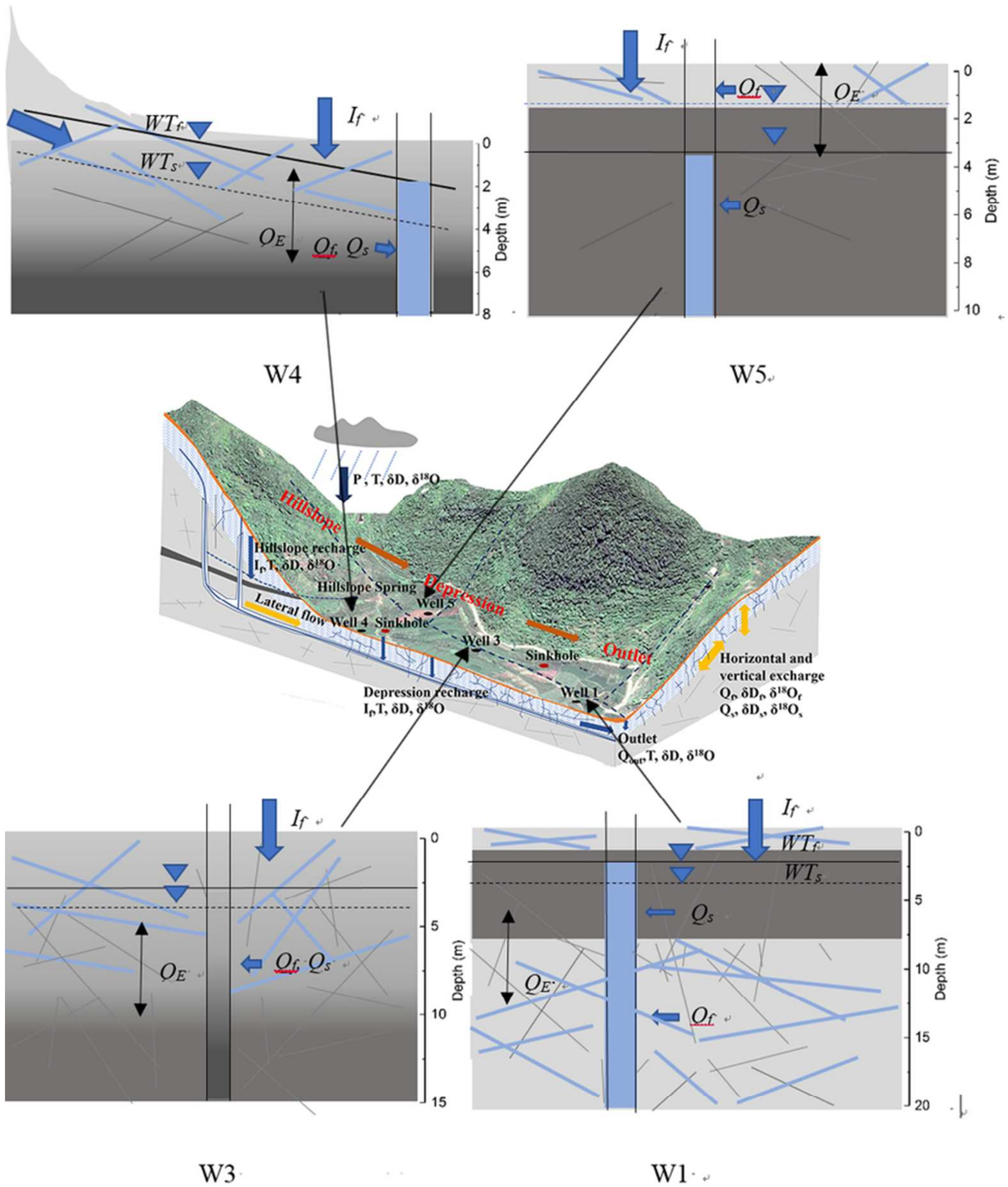

Figure 9 Conceptual model of groundwater aquifer at depression wells of W1, W3, W4 and W5. The high permeability layers in the grey color areas and low permeability layers in the deep grey color areas. WTf on solid lines is water table of fast flow reservoir, WTs on dotted lines is water table of slow flow reservoir, QE is exchange flow between fast (Qf) and slow flow (Qs) reservoirs and If is rainfall recharge.

36x43mm (600 x 600 DPI)